End-binding proteins EB3 and EB1 link microtubules to ankyrin G in the axon initial segment

Christophe Leterrier, Hélène Vacher, Marie-Pierre Fache, Stéphanie Angles d'Ortoli, Francis Castets, Amapola Autillo-Touati, Bénédicte Dargent

End-binding proteins EB3 and EB1 link microtubules to ankyrin G in the axon initial segment

Christophe Leterrier[a,b], Hélène Vacher[a,b], Marie-Pierre Fache[a,b], Stéphanie Angles d'Ortoli[a,b], Francis Castets[a,b], Amapola Autillo-Touati[a,b], and Bénédicte Dargent[a,b,1]

[a]Institut National de la Santé et de la Recherche Médicale, Unité Mixte de Recherche 641, F-13916 Marseille, France; and [b]Faculté de Médecine Secteur-Nord, Institut Fédératif de Recherche Jean Roche, Université de la Méditerranée, F-13916 Marseille, France

Edited* by Vann Bennett, Duke University Medical Center, Durham, NC, and approved April 7, 2011 (received for review December 13, 2010)

The axon initial segment (AIS) plays a key role in maintaining the molecular and functional polarity of the neuron. The relationship between the AIS architecture and the microtubules (MTs) supporting axonal transport is unknown. Here we provide evidence that the MT plus-end-binding (EB) proteins EB1 and EB3 have a role in the AIS in addition to their MT plus-end tracking protein behavior in other neuronal compartments. In mature neurons, EB3 is concentrated and stabilized in the AIS. We identified a direct interaction between EB3/EB1 and the AIS scaffold protein ankyrin G (ankG). In addition, EB3 and EB1 participate in AIS maintenance, and AIS disassembly through ankG knockdown leads to cell-wide up-regulation of EB3 and EB1 comets. Thus, EB3 and EB1 coordinate a molecular and functional interplay between ankG and the AIS MTs that supports the central role of ankG in the maintenance of neuronal polarity.

Neurons are highly polarized cells that rely on microtubules (MTs) for maintenance of their architecture and long-range polarized trafficking (1). MTs supporting axonal transport travel through the axon initial segment (AIS), a compartment that is essential for the generation of action potentials (2) and the maintenance of neuronal polarity (3). Generation of action potentials depends on the concentration of voltage-gated sodium (Nav) and potassium channels at the AIS, which are tethered at the plasma membrane via their interaction with ankyrin G (ankG (4–7). ankG, in turn, is linked to the actin cytoskeleton via βIV-spectrin and organizes AIS formation by recruiting membrane proteins and βIV-spectrin to the nascent AIS (3).

The AIS maintains neuronal polarity by forming a diffusion barrier for membrane constituents at the cell surface (4, 8, 9) and also by dampening intracellular diffusion and vesicular transport through the AIS (10). Both phenomena depend on ankG, because depletion of ankG results in the disappearance of AIS and the acquisition of dendritic identity by the proximal axon (11, 12). However, the molecular role of ankG in the intracellular AIS organization is still unknown. The dependence of the AIS intracellular filter on ankG (10) and the disorganization of MT bundles in the AIS of Purkinje cells from ankG-deficient mice (12) suggest an unknown link between ankG and MTs in the AIS.

The end-binding (EB) proteins family, composed of three members (EB1–3), has been described as plus-end–tracking proteins (+TIPs) that coordinate a network of dynamic proteins on the growing MT plus-ends (13). In neurons, EB1 has been implicated in axonal transport (14, 15), whereas EB3 has been characterized as a molecular link between MTs and the actin cytoskeleton (16, 17). We hypothesized that EB proteins could have a role in the AIS via interaction with the ankG/βIV-spectrin scaffold. We first found that EB3 is accumulated and stabilized in the AIS of mature neurons. Both EB3 and EB1 bind to ankG and participate in the maintenance of the AIS scaffold. Reciprocally, altering neuronal polarity through ankG knockdown induces a cell-wide up-regulation of EB3 and EB1 comets. Thus, the EB protein link between MTs and ankG provides a molecular insight into how the AIS scaffold and MTs are organized and could contribute to the maintenance of neuronal polarity.

Results

EB3 Concentrates in the AIS of Mature Neurons. We first assessed the localization of EB3 in cultured rat hippocampal neurons. In mature neurons, EB3 was present as puncta bound to MT plus-ends throughout the soma and dendrites (17) and also concentrated in the AIS with alignments of closely apposed or overlapping aggregates (Fig. 1*A*). In our cultures, EB3 expression increased after 10 d in vitro (div) (Fig. S1; also see Fig. 5*A*) (17), and enrichment in the AIS was detected as soon as individual neurons started expressing EB3 (Fig. 1*B* and Fig. S1). Consistently, the ratio of EB3 intensity in the AIS to that in dendrites (AIS/D) was greater than 1 at all examined ages (Fig. 1*C*). EB proteins recruit +TIP partners such as cytoplasmic linker proteins (CLIPs) and CLIP-associated proteins (CLASPs) to MT plus-ends (13), suggesting that these downstream +TIPs also could be concentrated in the AIS. CLIP170 and CLASP1/2 were immunostained in mature cultured neurons, but their presence or enrichment in the AIS was not observed (Fig. 1*D* and Fig. S2). This result indicates that EB3 in the AIS could be part of a complex distinct from the classical MT plus-ends assembly.

Stable, MT-Dependent Concentration of EB3 in the AIS. As a +TIP, EB proteins concentrate as transient comets at the growing MT plus-ends (18). To compare the dynamic behavior of EB3 in the AIS and in dendrites, we transfected EB3-GFP in 8- to 10-div neurons followed by live-cell imaging using highly inclined illumination microscopy (Fig. 2*A* and Movie S1). In the cell body and dendrites, we observed numerous mobile, transient EB3-GFP comets. Strikingly, EB3-GFP enriched in the AIS was mostly immobile, with very few comets detectable inside the AIS (Fig. 2*A* and Movie S1). To probe the stability of EB3 in the AIS directly and to verify that EB3 enrichment was not masking mobile EB3 comets, we performed fluorescence recovery after photobleaching (FRAP) analysis of EB3-GFP in the AIS and dendrites of 8- to 10-div neurons. In the AIS, we never observed comets invading the bleached area, suggesting that EB3 enrichment in the AIS is not caused by an accumulation of MT plus-ends (Fig. S3). Recovery of fluorescence was more incomplete in the AIS than in dendrites (Fig. 2*B*), revealing the accumulation of an immobilized population of EB3 in the AIS (Fig. 2*C*). This concentration and stabilization of EB3 in the AIS probably involves an association of EB3 along the MT lattice. Thus, we assessed EB3 localization in 21-div neurons after acute (2 h) nocodazole and taxol treatments that perturb MTs (Fig. 2*D*). A low-dose (0.2 μM) nocodazole treatment that abolished MT dynamics was sufficient to induce the disappearance of the EB3 somatodendritic puncta and re-

Author contributions: C.L., H.V., and B.D. designed research; C.L., H.V., M.-P.F., and S.A.dO. performed research; F.C. and A.A.-T. contributed new reagents/analytic tools; C.L., H.V., M.-P.F., and S.A.dO. analyzed data; and C.L. and B.D. wrote the paper.

The authors declare no conflict of interest.

*This Direct Submission article had a prearranged editor.

[1]To whom correspondence should be addressed. E-mail: benedicte.dargent@univmed.fr.

This article contains supporting information online at www.pnas.org/lookup/suppl/doi:10.1073/pnas.1018671108/-/DCSupplemental.

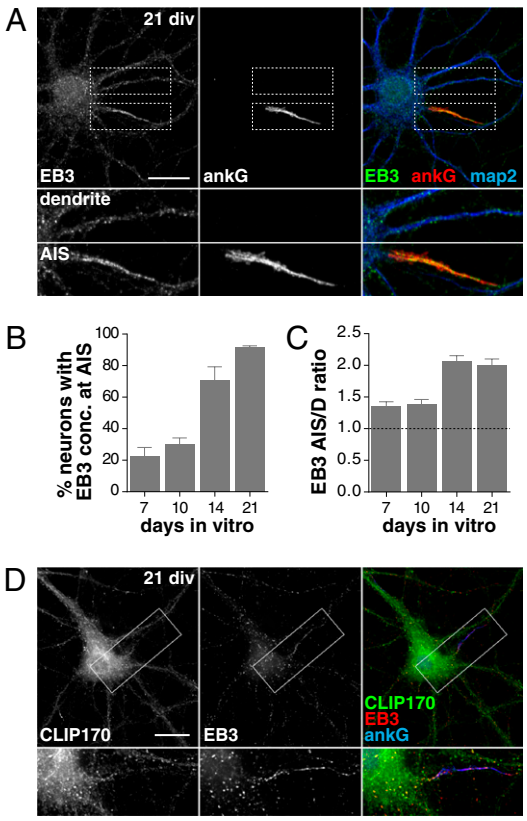

Fig. 1. Concentration of EB3 in the AIS of neurons. (*A*) EB3 (green) colocalizes with ankG (red) and concentrates in the AIS of 21-div hippocampal neurons. Microtubule-associated protein 2 (map2) is shown in blue. (Scale bar: 20 μm.) (*B*) Time course of the percentage of cells that exhibit EB3 concentrated in the AIS during neuronal maturation. Bars indicate mean ± SEM; n = 307–620 neurons from three to five independent experiments. (*C*) Time course of the EB3 mean intensity ratio between the AIS and proximal dendrites (AIS/D ratio). Bars indicate mean ± SEM; n = 47 or 48 neurons from three experiments. (*D*) Localization of CLIP170 in 21-div hippocampal neurons. CLIP170, green; EB3, red; ankG, blue. (Scale bar: 10 μm.)

duced overall EB3 labeling intensity (17). EB3 enrichment in the AIS still was detected in most neurons after this treatment, indicating that EB3 accumulation does not depend on MT plus-end dynamics (Fig. 2*E*). By contrast, altering the assembled MTs using a high dose (20 μM) of nocodazole (17) or stabilizing all MTs using taxol (0.2 μM) disrupted AIS enrichment of EB3 in half the neurons (Fig. 2*E*), and high-dose nocodazole was able to alter the average AIS/D ratio for EB3 labeling significantly (Fig. 2*F*). These observations strongly suggest that EB3 stabilization depends on the integrity and stability of the MT lattice.

EB3 Binds Directly to AnkG. The concentration and stability of EB3 in the AIS suggest that it is linked to the ankG scaffold. To test the interaction of EB3 with ankG, we first performed GST pulldown assays with bacterially expressed GST-EB3 and either ankG-GFP or ankB-GFP transfected in COS cells. AnkG was able to bind to recombinant EB3, but ankB, the other neuronal ankyrin expressed along distal axons, could not (Fig. 3*A* and Fig. S4) (19). We next used surface plasmon resonance (SPR) experiments to assess the direct interaction between EB3 and ankG. Purified 190-kDa ankG bound to GST-EB3 with nanomolar affinity (K_d = 1.2 ± 0.7 nM), whereas no binding was observed for 220-kDa ankB (Fig. 3*B* and Table S1). To confirm the EB3–ankG interaction in a cellular context, we used a cell-based MT recruitment assay. In COS cells, ankG-mCherry (ankG-mCh) showed an homogeneous submembrane localization (Fig. 3*C*). Overexpressed EB3-GFP accumulated along MTs, inducing MT bundles (20). When coexpressed with EB3-GFP, ankG-mCh was recruited to MTs in 47 ± 6% of cells with high EB3-GFP expression, compared with 4 ± 3% of cells transfected with ankG-mCh and tubulin-GFP (Fig. 3 *D* and *E*). Moreover, HA-tagged EB3 also recruited ankG-GFP, but not ankB-GFP, to MTs (Fig. 3*E* and Fig. S5 *A*–*C*), confirming the specificity of the EB3–ankG interaction. Binding of EB3 to MTs is necessary for the recruitment of ankG in this assay, because a truncated EB3 lacking the MT-binding 195-amino acid terminal residues (EB3Δ*N*-GFP) still was able to bind ankG (Fig. S4) but did not associate with MTs and did not recruit ankG-mCherry (Fig. S5*D*).

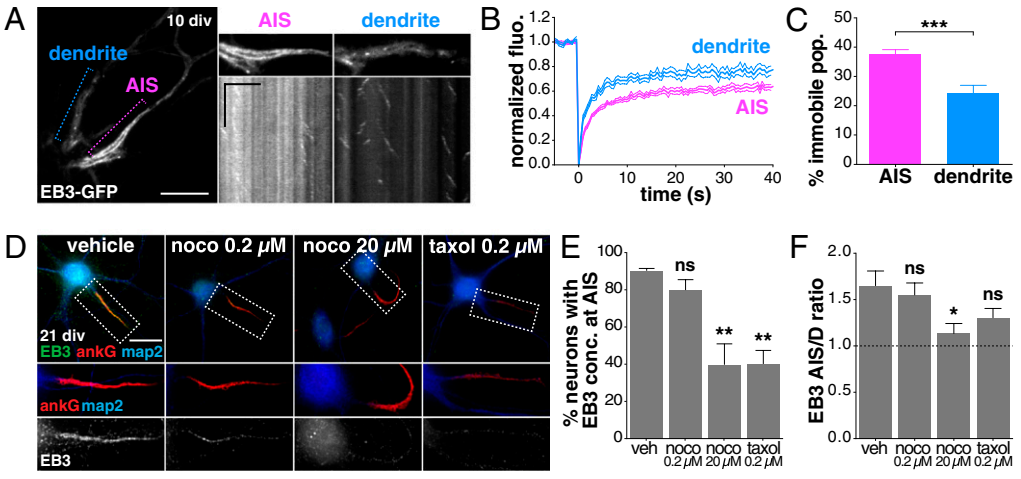

Fig. 2. EB3 is immobile and stabilized at the AIS. (*A*) Live-cell imaging of a 10-div neuron transfected with EB3-GFP (Movie S1). The kymograph along the AIS (purple) shows the concentration of EB3 with no discernable comet movement. The kymograph along a dendrite (blue) reveals the bidirectional movement of several comets. [Scale bars: 10 μm (*Left*); 5 μm (*Right* and horizontal kymograph direction in *Center*); 60 s (vertical kymograph direction in *Center*). (*B*) Normalized mean fluorescence recovery curves for point FRAP experiments on 8- to 9-div neurons expressing EB3-GFP. Recovery is less complete in the AIS (purple) than in dendrites (blue). Mean (thick line) ± SEM (thin line), n =14 neurons from two experiments. (*C*) Percentage of immobile EB3-GFP population in the AIS and dendrites calculated from individual recovery curves. Bars indicate mean ± SEM; n = 19 neurons from two experiments; t test; ***P < 0.001. (*D*) Effect of MT perturbations on EB3 localization in 21-div neurons. Nocodazole (noco) (0.2 μM or 20 μM for 2 h) or taxol (0.2 μM for 2 h) induces a disappearance of the EB3 somatodendritic puncta (EB3, green; map2, blue) but only partially perturbs EB3 concentration in the AIS (ankG, red). (Scale bar: 20 μm.) (*E*) Percentage of neurons that exhibit EB3 concentration in the AIS after MT perturbations. veh, vehicle condition. Bars indicate mean ± SEM; n = 301–330 neurons from three experiments; one-way ANOVA posttest comparison with vehicle; **P < 0.01; nonsignificant (ns), P > 0.05. (*F*) AIS/D ratio for EB3 after MT perturbations. Bars indicate mean ± SEM; n = 35–36 neurons from three experiments; one-way ANOVA posttest comparison with vehicle, *P < 0.05; ns, P > 0.05.

NEUROSCIENCE

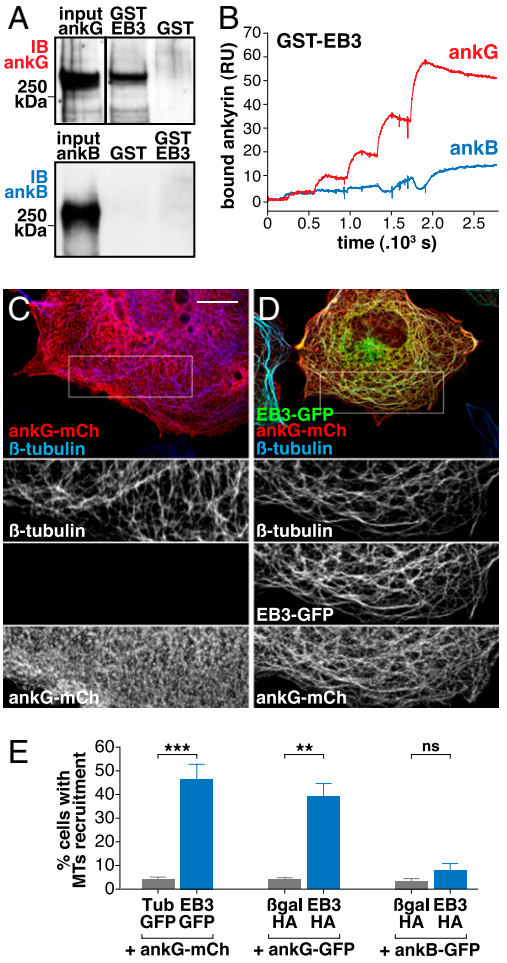

Fig. 3. EB3 interacts directly with ankG. (*A*) GST-EB3 pulls down ankG-GFP from transfected COS cell lysates [*Upper* (Fig. S4 shows full gel)] but ankB-GFP does not (*Lower*), as shown by immunoblotting (IB). (*B*) Representative SPR curves: Purified 190-kDa ankG (red), but not 220-kDa ankB (blue), binds to immobilized GST-EB3. (Quantitative parameters are given in Table S1.) (*C*) COS cell recruitment assay: ankG-mCh (red) shows a submembrane localization when transfected in COS cells. (Scale bar: 20 μm.) (*D*) Coexpression of EB3-GFP (green) induces recruitment of ankG to MTs identified by β-tubulin staining (blue). (*E*) Percentage of COS cells with recruitment of ankyrin to MTs, showing preferential recruitment of ankG over ankB by EB3-HA. Bars represent mean ± SEM; n = 256–1,403 cells from two to seven experiments; one-way ANOVA posttest comparison; $^{***}P < 0.001$, $^{**}P < 0.01$, ns $P > 0.05$.

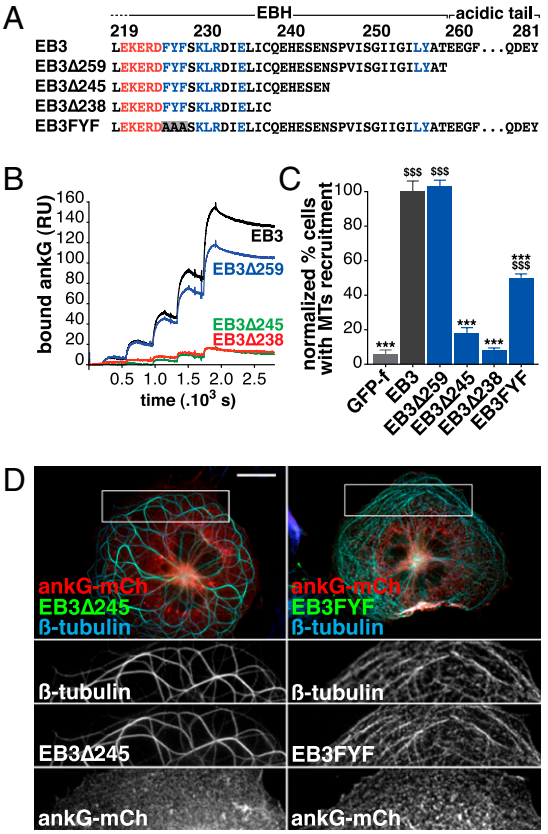

Fig. 4. AnkG binds to the EBH-domain hydrophobic pocket of EB3. (*A*) Amino acid sequence of the C terminus for EB3 mutant constructs. In the EBH domain, highlighted features are the polar rim (amino acids in red) and the hydrophobic pocket (amino acids in blue). (*B*) Representative SPR curves for 190-kDa ankG binding to GST-EB3 truncated constructs: EB3Δ245 and EB3Δ238 fail to bind ankG. (Quantitative parameters are given in Table S1.) (*C*) Quantification of ankG-mCh recruitment to MTs by EB3-GFP mutants: percentage of COS cells showing recruitment of ankG to MTs, normalized to the recruitment effect of full-length EB3. EB3Δ259 is able to recruit ankG to MTs, but EB3Δ245 and EB3Δ238 are not, and EB3FYF is only partially competent for ankG recruitment. Bars indicate mean ± SEM; n = 300 cells from three experiments; one-way ANOVA posttest comparison with GFPf ($^{\$\$\$}P < 0.001$) or with full-length EB3 ($^{***}P < 0.001$). (*D*) Representative images of cells expressing EB3Δ245 (green, *Left*) or EB3FYF (green, *Right*) that fail to recruit ankG-mCh (red) to MTs (blue). (Scale bar: 20 μm.)

AnkG Binds to the End-Binding Homology Domain Hydrophobic Pocket of EB3. To characterize the ankG-binding site on EB3, we generated several truncated mutants of the EB3 C terminus, which consists in an end-binding homology (EBH) domain and an acidic tail (Fig. 4*A*). The EBH domain contains a polar rim followed by a hydrophobic pocket that is important for the binding of EB protein-interacting +TIPs (21). We first evaluated the ability of truncated EB3 constructs to interact with ankG in SPR experiments. EB3Δ259 still bound to ankG with a nanomolar affinity, but EB3Δ245 and EB3Δ238 did not bind to ankG (Fig. 4*B* and Table S1). In COS cell assays, EB3Δ259-GFP recruited ankG-mCh to MTs, but EB3Δ245-GFP and EB3Δ238-GFP did not (Fig. 4 *C* and *D* and Fig. S6). Taken together, these findings suggest that EB3 residues between positions 245–259 are critical for ankG binding. These residues encompass the last part of the hydrophobic pocket (22). Therefore, we abrogated the other extremity of the hydrophobic pocket by replacing the FYF at positions 225–227 by an alanine stretch. AnkG recruitment to MTs was altered in cells expressing EB3FYF-GFP (Fig. 4 *C* and *D*). Thus, ankG binds to the hydrophobic pocket in the EBH domain of EB3, the same site used by other EB protein +TIPs partners. This competitive binding by ankG might explain the exclusion of other +TIPs observed in the AIS (Fig. 1*D* and Fig. S2).

EB1 Is Expressed in Mature Neurons and Binds to AnkG. Importantly, the ankG-binding site on EB3 is conserved across the three members of the EB protein family (22). We thus wondered if EB1 and EB2 also could have a role in the AIS of neurons. Western blots revealed that EB1 and EB2 are expressed at all ages in maturating cultures. In contrast, EB3 expression was low in immature neurons and increased after 10 div (Fig. 5*A*). Simultaneous immunolabeling for EB3 and EB1 showed that EB3 levels increased with respect to EB1 during neuronal maturation (Fig. 5*B*). In mature neurons, EB2 was present mostly in the cell body and axons but never was enriched in the AIS (Fig. S7) (17). In contrast, EB1 localizes in somatic puncta and along axons (15), with accumulation in the AIS for a subpopulation of neurons, as previously observed (Fig. 5*C*) (14). This subcellular localization prompted us

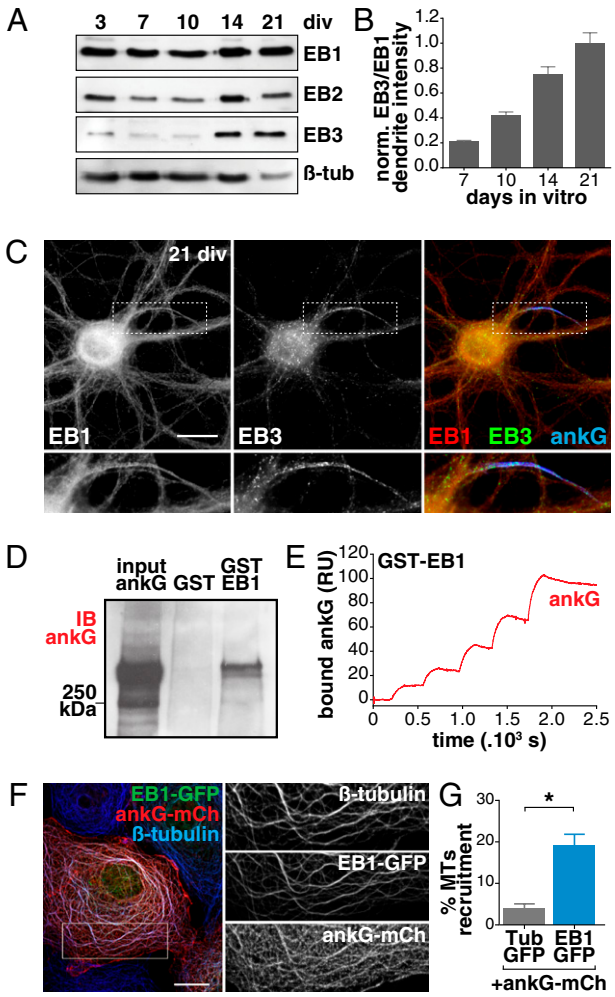

Fig. 5. EB1 is expressed in mature neurons and binds to ankG. (*A*) Western blot showing the developmental expression of members of the EB protein family in cultured hippocampal neurons. (*B*) EB3/EB1 immunolabeling ratios during neuronal culture maturation. Mean intensities of EB1 and EB3 labeling were measured along proximal dendrites, and ratios were normalized to the ratio reached at 21 div. (*C*) Example of a 21-div neuron showing an enrichment of EB1 (red) in the AIS. (EB3 is shown in green and ankG in blue.) (Scale bar: 20 μm.) (*D*) GST-EB1 pulls down ankG-GFP from transfected COS cell lysates. (*E*) Representative SPR curve: purified 190-kDa ankG binding to GST-EB1. (Quantitative parameters are given in Table S1.) (*F*) In COS cells, EB1-GFP (green) is able to recruit ankG-mCh (red) on MTs. (Scale bar: 20 μm.) (*G*) Percentage of COS cells that show recruitment of ankyrin to MTs when coexpressed with tubulin-GFP (Tub-GFP) or EB1-GFP. Bars indicate mean ± SEM; n = 535–1,403 cells from three to seven experiments; t test; $^*P < 0.05$.

to examine the possible binding of EB1 to ankG. GST-EB1 was able to interact with ankG-GFP in GST pulldown assays (Fig. 5*D*). SPR experiments confirmed that EB1 interacts directly with ankG with a nanomolar affinity ($K_d = 1.4 \pm 0.9$ nM), similar to EB3 (Fig. 5*E* and Table S1). Last, EB1-GFP was able to recruit ankG-mCh on MTs when coexpressed in COS cells (Fig. 5 *F* and *G*). These results indicate that, although EB3 is the predominant EB protein present in the AIS of mature neurons, EB1 also is likely to play a role as a link between ankG and MTs. The hydrophobic pocket sequence is higly conserved between the three EB family members, suggesting that ankG binds to EB1 through the same binding site as EB3, and that ankG also could bind to EB2.

Functional Interplay Among EB3, EB1, and the AIS Scaffold. To unravel the functional role of the EB protein–ankG interaction, we knocked down EB3 and EB1 in hippocampal cultures from 10–16 div and assessed ankG accumulation in the AIS. Transfection of shRNA plasmids containing previously validated shRNA sequences against EB3 and EB1 (17, 23) together with a plasmid expressing farnesylated GFP (GFPf) was able to deplete target proteins in cultured neurons efficiently, as revealed by immunolabeling (Fig. 6*C*). AnkG concentration was reduced in neurons depleted for EB3 as compared with neurons transfected with a control plasmid lacking the shRNA cassette (Fig. 6 *A* and *D* and Fig. S8*A*; ratio of AIS intensity in the transfected neuron to that in surrounding nontransfected cells, 0.72 ± 0.03 for shEB3, 1.00 ± 0.03 for control, ANOVA, $P < 0.001$). Furthermore, AIS concentration of Nav channels, which depend on ankG anchoring (6, 11), also was reduced after EB3 knockdown (Fig. 6*D* and Fig. S8*B*; ratios of AIS intensity 0.61 ± 0.05 for shEB3 and 1.01 ± 0.05 for control, ANOVA, $P < 0.001$). Interestingly, EB1 knockdown also decreased ankG concentration in the AIS (Fig. 6 *B* and *D*; ratio of AIS intensity 0.86 ± 0.04 for shEB1, ANOVA, $P < 0.001$), but the effect was significantly lower than for EB3 depletion.

AnkG knockdown has been shown to destabilize all tested AIS constituents and to affect proximal axon molecular identity (11). Therefore, we evaluated the effect of ankG depletion and the consequent AIS disassembly on EB3 and EB1 distribution in neurons. Strikingly, ankG knockdown led to a strong up-regulation of EB3 with an increased number of bright puncta in the soma and dendrites (Fig. 6 *E* and *G*; ratios of soma intensity 1.00 ± 0.04 for control and 2.7 ± 0.16 for shAnkG, ANOVA, $P < 0.001$). Because of the scarcity of transfected neurons in cultures, we could not measure the up-regulation of EB3/EB1 expression directly by Western blotting. AnkG knockdown also up-regulated EB1 expression, albeit to a lesser extent (Fig. 6 *F* and *G*; ratios of soma intensity 1.00 ± 0.05 for control and 1.5 ± 0.11 for shAnkG, ANOVA, $P < 0.001$). This up-regulation effect suggests that EB3/EB1 expression and localization is tightly coupled to the presence of an intact AIS scaffold.

Discussion

The AIS is the checkpoint between the somatodendritic and axonal compartments, ensuring final integration of dendritic inputs, generation of action potentials, and maintenance of the neuronal polarity (3). The role of ankG as an organizer of AIS membrane proteins now is well characterized (6, 9, 24). However, how the AIS maintains polarity through its intracellular organization is unknown. Here, we identified EB proteins as molecular links between MTs and the ankG scaffold in the AIS. EB3 concentrates at the AIS of mature neurons, where it is stably associated along the MT lattice. EB3 and EB1 interact directly and with a high affinity with ankG. AnkG binds to EB3 in the EBH-domain hydrophobic pocket, suggesting that ankG capture competes with +TIP binding and defines a specific role for EB proteins in the AIS. Finally, EB3 and EB1 reciprocally stabilize the AIS architecture and the MT network, because depletion of EB3/EB1 impairs AIS integrity, whereas depletion of ankG leads to a cell-wide up-regulation of MT dynamics and EB3/EB1 expression.

EB proteins have been characterized as core +TIPs, organizing a molecular complex around growing MT plus-ends that dynamically explore the cytoplasm and interact with organelles and the cell cortex (21). We have found that EB proteins have a distinct behavior in the AIS, in contrast to their +TIP role in other neuronal compartments. First, accumulation of EB3 in the AIS results from the immobilization of a fraction of the EB3 population. This stabilization probably reflects association along the AIS MT lattice rather than a dynamic accumulation of MT plus-ends, as indicated by the FRAP and MT perturbation experiments. This result is consistent with the findings of Nakata et al. (25) showing that transfected EB1-GFP can bind along the MT lattice in the AIS. Second, the ankG-binding site on EB3 also is used by EB protein-binding +TIPs, and the absence of +TIP partners in the AIS

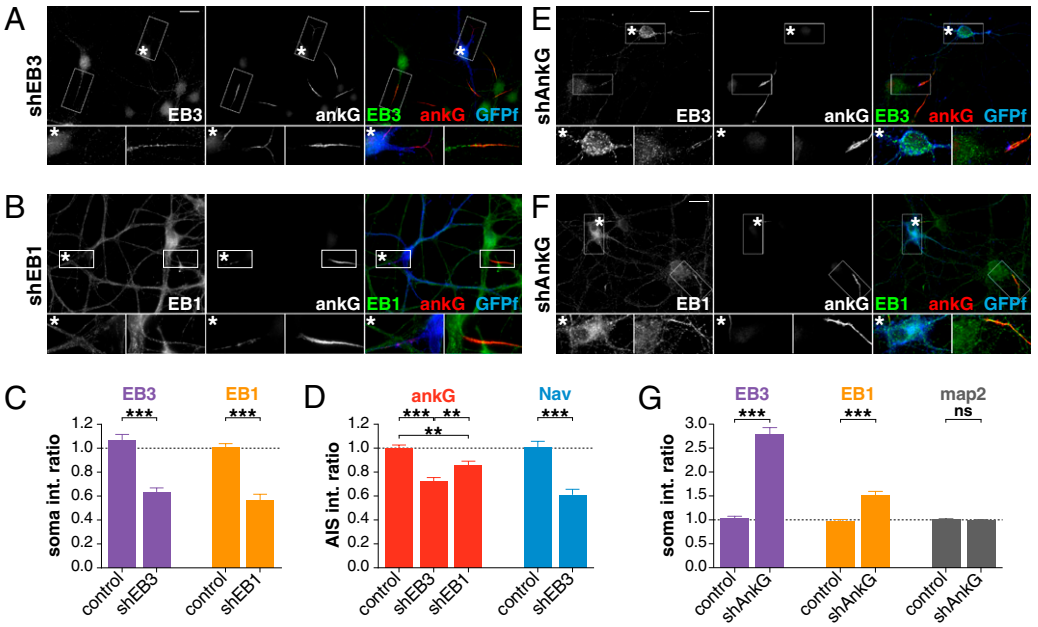

Fig. 6. Functional interplay between EB3/EB1 and ankG in hippocampal neurons. (*A*) After 6 d of EB3 knockdown, 16-div neurons show a decreased concentration of ankG in the AIS of a transfected neuron (asterisk-labeled boxes) compared with nontransfected neurons (unlabeled boxes). EB3 is shown in green, ankG in red, and GFPf in blue. (Scale bar: 20 μm.) (*B*) EB1 knockdown also alters the concentration of ankG in the AIS. EB1 is shown in green, ankG in red, and GFPf in blue. (Scale bar: 20 μm.) (*C*) Quantification of the soma intensity ratio (soma int. ratio; i.e., the ratio of the intensity of the transfected neuron to the intensity of the surrounding nontransfected cells) of neurons transfected with control or shEB3 plasmid and labeled for EB3. Bars indicate mean ± SEM; n = 24–58 neurons from three to five experiments; one-way ANOVA posttest comparison; ***$P < 0.001$. (*D*) Quantification of the AIS intensity ratio (AIS int. ratio) of neurons transfected with control, shEB3, or shEB1 plasmid and labeled for ankG or Nav. Bars represent mean ± SEM; n = 19–116 neurons from two to seven experiments; one-way ANOVA posttest comparison; ***$P < 0.001$, **$P < 0.01$. (*E*) AnkG knockdown up-regulates EB3 puncta in the soma and dendrites. EB3 is shown in green, ankG in red, and GFPf in blue. (Scale bar: 20 μm.) (*F*) AnkG knockdown also up-regulates EB1 puncta, but to a lesser extent. EB1 is shown in green, ankG in red, and GFP in blue. (Scale bar: 20 μm.) (*G*) Quantification of the soma intensity ratio of neurons transfected with control or shAnkG plasmid and labeled for EB3, EB1, or map2. Bars indicate mean ± SEM; n = 81–167 neurons from three to seven experiments; one-way ANOVA posttest comparison; ***$P < 0.001$, ns, $P > 0.05$.

suggests that they could be excluded by ankG binding to EB proteins. The ankG–EB protein complex therefore appears to be distinct from the EB protein complex at MT plus-ends, indicating functional specificity.

What is the function of the stable EB protein–ankG complex in the AIS? MTs traveling through the AIS are the only tracks for axonal delivery, so their stability probably contributes to the robustness of axonal trafficking. We propose that ankG also participates in such stabilization by capturing EB proteins along MTs. EB protein-decorated MT bundles are more resistant to depolymerization (20). Moreover, MTs linked to ankG could benefit from the remarkable structural stability of the AIS scaffold (11). EB proteins stabilized along the AIS also could function as a trafficking cue for vesicular transport to the axon (25). Kinesins implicated in axonal transport have been shown to recognize the axonal entrance by preferentially binding to stabilized MTs (26). It would be interesting to assess whether EB proteins participate in such a preferential recruitment through MT stability and motor protein affinities. Finally, the interplay between the ankG scaffold and MT stability extends beyond the AIS. Depletion of ankG in neurons had a dramatic effect on the expression of EB proteins, with the appearance of numerous EB3/EB1 puncta in the soma and dendrites of ankG-deficient neurons. It would be interesting to extend this observation by studying the effect of other AIS perturbations, because it suggests a massive effect of AIS disassembly on MT dynamics at the whole-cell level. Interestingly, up-regulation of EB proteins caused by ankG depletion is similar to the effect of in vivo axotomy in *Drosophila* neurons (27), demonstrating the profound consequences of AIS disassembly on neuronal polarity.

Our identification of EB3 and EB1 as links between MTs and ankG is a significant advance in the understanding of the AIS architecture. At the molecular level, the extension of ankG (0.5–1 μm) (28) could allow ankG to link physically MT bundles (via EB proteins) and submembrane actin (via βIV-spectrin). This organization suggests a structural basis for the ankG-dependent diffusion and trafficking filter that assembles at the AIS during neuronal maturation (10). Furthermore, the connection between MTs and actin via EB protein/ankG/βIV-spectrin highlights the importance of ankG as a multifunctional scaffold that assembles and maintains the AIS structure. Analogous to this EB protein-mediated interaction, the links between ankyrin-based scaffolds and the MT cytoskeleton probably also have important roles in other highly differentiated cells such as muscle or epithelial cells (28).

Materials and Methods

Details of plasmid constructs, recombinant proteins, and antibodies used in this study can be found in *SI Materials and Methods*. Procedures for Western blotting and GST pulldown assays also can be found in *SI Materials and Methods*.

SPR. SPR experiments were performed at 25 °C on a Biacore 3000 instrument (GE Healthcare) with CM5 sensor chips, using HBS-EP running buffer (GE Healthcare). Approximately 5–18 fmol of GST fusion proteins and GST were immobilized in flow cells via anti-GST polyclonal goat antibody covalently coupled using amine-coupling chemistry. The single-cycle kinetic method (29) was used to analyze the binding of ankB (220 kDa) or ankG (190 kDa) to captured GST fusions of EB3, EB3 mutants, and EB1. Additional details are given in *SI Materials and Methods*.

Animals. The use of Wistar rats followed the guidelines established by the European Animal Care and Use Committee (86/609/CEE) and was approved by the local ethics committee (agreement C13-055-8).

Cell Culture and Transfection. COS-1 and COS-7 cells were cultured as described previously (6), transfected using Lipofectamine 2000 (Invitrogen) according to the manufacturer's instructions, and fixed 24 h after transfection. Rat hippocampal neurons were cultured as described (6), transfected using Lipofectamine 2000, and fixed at the indicated time points.

Immunofluorescence. COS cells were fixed with cold MeOH for 7 min. Neuronal cells were fixed with MeOH at −20 °C for 5 min followed by 4% paraformaldehyde for 5 min and were processed for immunocytochemistry as previously described (4). Additional details are given in *SI Materials and Methods*.

Microscopy, Image Acquisition, and Processing. Imaging of cultured cells was carried out using an AxioObserver microscope (Zeiss) fitted with a QuantEM camera (Photometrics) and piloted by either MetaMorph (Molecular Devices) or AxioVision (Zeiss). A 40×, NA 1.2 oil objective and appropriate fluorescence filters were used for COS cell or neuron counts and quantification. The AIS/D ratio is the ratio of the mean intensity along the AIS and the mean intensity along proximal dendrites for a given neuron. The AIS (soma) intensity ratio for one image is defined as the mean intensity of the AIS (soma) for a transfected neuron divided by the average of the mean intensities of the AIS (somas) of all surrounding nontransfected neurons. For shRNA experiments, this ratio was compared in neurons transfected with the shRNA plasmid and in neurons with a control plasmid lacking the shRNA cassette. Additional details are given in *SI Materials and Methods*.

Live Cell Imaging and FRAP Experiments. Neurons were transfected at 7–10 div and imaged 24–48 h after transfection. Imaging was carried out using an AxioObserver microscope (Zeiss). We used a 488-nm laser (Errol) through a 100× total internal reflection fluorescence (TIRF) objective in highly inclined illumination mode (25) to image up to ∼0.5–1 μm from the glass substrate. FRAP experiments were performed using a spinning-disk system (Yokogawa CSU22) combined with a laser-scanning FRAP system (Roper Scientific). Point regions (1-μm diameter) were bleached (by 60–70%), and background-corrected, normalized curves were used for recovery quantification. Additional details are given in *SI Materials and Methods*.

Statistical Analysis. Statistical analyses were performed using Prism (Graphpad Software). Significance of the differences was assessed using a two-tailed *t* test or one-way ANOVA followed by Dunnett or Newman–Keuls posttest.

ACKNOWLEDGMENTS. We thank F. Rueda, G. Caillol, and A. Tasmadjian for technical help; A. Woodhouse for critically reading the manuscript; C. Lévêque and G. Ferracci for help with the SPR experiments; D. Choquet, C. Breillat and C. Poujol for help with FRAP experiments; and V. Bennett, A. Akhmanova, M. Coppey, P. Gordon-Weeks, A. Benmerah, C. Berlot, C. Hoogenraad, R. Tsien, F. Watrin, and N. Galjart for sharing antibodies, recombinant proteins, and plasmids. This work was supported by the Institut National de la Santé et de la Recherche Médicale, the Centre National pour la Recherche Scientifique, and by Grant A05161from the Agence Nationale pour la Recherche, Grant R06048AA from the Fondation pour la Recherche Médicale, Grant IRG-2008-239499 from the Marie Curie 7th Framework Program (to H.V.), and grants from the National Multiple Sclerosis Society and the Fondation pour l'Aide à la Recherche sur la Sclérose En Plaques (to C.L.).

1. Kapitein LC, Hoogenraad CC (2011) Which way to go? Cytoskeletal organization and polarized transport in neurons. *Mol Cell Neurosci* 46:9–20.
2. Clark BD, Goldberg EM, Rudy B (2009) Electrogenic tuning of the axon initial segment. *Neuroscientist* 15:651–668.
3. Rasband MN (2010) The axon initial segment and the maintenance of neuronal polarity. *Nat Rev Neurosci* 11:552–562.
4. Brachet A, et al. (2010) Ankyrin G restricts ion channel diffusion at the axonal initial segment before the establishment of the diffusion barrier. *J Cell Biol* 191:383–395.
5. Bréchet A, et al. (2008) Protein kinase CK2 contributes to the organization of sodium channels in axonal membranes by regulating their interactions with ankyrin G. *J Cell Biol* 183:1101–1114.
6. Garrido JJ, et al. (2003) A targeting motif involved in sodium channel clustering at the axonal initial segment. *Science* 300:2091–2094.
7. Kole MHP, et al. (2008) Action potential generation requires a high sodium channel density in the axon initial segment. *Nat Neurosci* 11:178–186.
8. Winckler B, Forscher P, Mellman I (1999) A diffusion barrier maintains distribution of membrane proteins in polarized neurons. *Nature* 397:698–701.
9. Nakada C, et al. (2003) Accumulation of anchored proteins forms membrane diffusion barriers during neuronal polarization. *Nat Cell Biol* 5:626–632.
10. Song A-H, et al. (2009) A selective filter for cytoplasmic transport at the axon initial segment. *Cell* 136:1148–1160.
11. Hedstrom KL, Ogawa Y, Rasband MN (2008) AnkyrinG is required for maintenance of the axon initial segment and neuronal polarity. *J Cell Biol* 183:635–640.
12. Sobotzik J-M, et al. (2009) AnkyrinG is required to maintain axo-dendritic polarity in vivo. *Proc Natl Acad Sci USA* 106:17564–17569.
13. Akhmanova A, Steinmetz MO (2008) Tracking the ends: A dynamic protein network controls the fate of microtubule tips. *Nat Rev Mol Cell Biol* 9:309–322.
14. Vacher H, et al. (2011) Cdk-mediated phosphorylation of the Kvbeta2 auxiliary subunit regulates Kv1 channel axonal targeting. *J Cell Biol* 192:813–824.
15. Gu C, et al. (2006) The microtubule plus-end tracking protein EB1 is required for Kv1 voltage-gated K+ channel axonal targeting. *Neuron* 52:803–816.
16. Geraldo S, Khanzada UK, Parsons M, Chilton JK, Gordon-Weeks PR (2008) Targeting of the F-actin-binding protein drebrin by the microtubule plus-tip protein EB3 is required for neuritogenesis. *Nat Cell Biol* 10:1181–1189.
17. Jaworski J, et al. (2009) Dynamic microtubules regulate dendritic spine morphology and synaptic plasticity. *Neuron* 61:85–100.
18. Stepanova T, et al. (2003) Visualization of microtubule growth in cultured neurons via the use of EB3-GFP (end-binding protein 3-green fluorescent protein). *J Neurosci* 23:2655–2664.
19. Boiko T, et al. (2007) Ankyrin-dependent and -independent mechanisms orchestrate axonal compartmentalization of L1 family members neurofascin and L1/neuron-glia cell adhesion molecule. *J Neurosci* 27:590–603.
20. Bu W, Su LK (2001) Regulation of microtubule assembly by human EB1 family proteins. *Oncogene* 20:3185–3192.
21. Akhmanova A, Steinmetz MO (2010) Microtubule +TIPs at a glance. *J Cell Sci* 123:3415–3419.
22. Honnappa S, et al. (2009) An EB1-binding motif acts as a microtubule tip localization signal. *Cell* 138:366–376.
23. Komarova Y, et al. (2005) EB1 and EB3 control CLIP dissociation from the ends of growing microtubules. *Mol Biol Cell* 16:5334–5345.
24. Hedstrom KL, et al. (2007) Neurofascin assembles a specialized extracellular matrix at the axon initial segment. *J Cell Biol* 178:875–886.
25. Nakata T, Hirokawa N (2003) Microtubules provide directional cues for polarized axonal transport through interaction with kinesin motor head. *J Cell Biol* 162:1045–1055.
26. Konishi Y, Setou M (2009) Tubulin tyrosination navigates the kinesin-1 motor domain to axons. *Nat Neurosci* 12:559–567.
27. Stone MC, Nguyen MM, Tao J, Allender DL, Rolls MM (2010) Global up-regulation of microtubule dynamics and polarity reversal during regeneration of an axon from a dendrite. *Mol Biol Cell* 21:767–777.
28. Bennett V, Healy J (2009) Membrane domains based on ankyrin and spectrin associated with cell-cell interactions. *Cold Spring Harb Perspect Biol* 1:a003012.
29. Karlsson R, Katsamba PS, Nordin H, Pol E, Myszka DG (2006) Analyzing a kinetic titration series using affinity biosensors. *Anal Biochem* 349:136–147.

Supporting Information

Leterrier et al. 10.1073/pnas.1018671108

SI Materials and Methods

Plasmids. Ankyrin G-mCherry (ankG-mCh) was constructed from ankG-GFP by excision of eGFP and insertion of mCh from mCherry-N1 using SalI/NotI restriction sites. End-binding (EB) protein EB3-GFP and GST-EB3 truncations and mutants were generated using Quickchange mutagenesis (Stratagene). Plasmids expressing shRNA were generated by inserting hairpin sequences into empty mu6pro plasmid, using previously described target sequences for EB1 and EB3 (1) and for ankG (2). All generated constructs were verified by DNA sequencing.

The following plasmids were gifts: plasmids encoding rat 270-kDa ankG-GFP (3) and human 220-kDa ankB-GFP (4) (Vann Bennett, Duke University, Durham, NC); human EB3-GFP (5) and EB3-HA (6) (Anna Akhmanova, Erasmus Medical Center, Rotterdam); mouse EB1-GFP (7) (Maïté Coppey, Institut Jacques Monod, Paris); GST fusions of human EB3 and EB3ΔNTer (8) (Phillip Gordon-Weeks, King's College, London); farnesylated GFP (GFPf) (Alexandre Benmerah, Institut Cochin, Paris); membrane-targeted mCherry (mem-mCh) (Catherine Berlot, Weis Center for Research, Danville, PA); ß-galactosidase (ßgal)-HA (Casper Hoogenraad, Erasmus Medical Center, Rotterdam); mCherry-N1 (Roger Tsien, University of California, San Diego); empty mu6pro shRNA plasmid (Françoise Watrin, Plateforme de Post-Génomique de l'Institut de Neurobiologie de la Méditerranée, Marseille, France).

Antibodies and Reagents. Purified recombinant histidine-tagged rat 190-kDa ankG (9) and human 220-kDa ankB (10) were gifts from Vann Bennett (Duke University, Durham, NC). Anti-cytoplasmic linker protein (CLIP) 170 #2360 (11) and anti-CLIP-associated protein (CLASP) 2 #2358 (12) rabbit sera were gifts from Niels Galjart (Erasmus Medical Center, Rotterdam). Anti-EB3 rat monoclonal antibody clone KT36, anti-EB1 rat monoclonal antibody clone KT51, anti-adenomatous polyposis coli rat monoclonal antibody clone T45, anti-CLASP1 rat monoclonal antibody clone KT67, anti–microtubule-associated protein 2 (map2) chicken polyclonal antibody, and anti-GFP rabbit polyclonal antibody #ab290 were from Abcam. Extracellular anti–neurofascin-186 mouse monoclonal antibody clone A12/18 and anti-ankG mouse monoclonal antibody clone N106/65 were from NeuroMab. Anti-Nav mouse monoclonal antibody clone K58/35 was from Sigma-Aldrich. Anti-RFP rabbit polyclonal antibody was from Rockland. Anti-HA rat monoclonal antibody clone 3F10 was from Roche Applied Bioscience. Anti–β-tubulin (β-tub) mouse monoclonal antibody clone E7 was from the Developmental Studies Hybridoma Bank. Secondary antibodies conjugated to Alexa Fluor 488 and 555 were from Invitrogen; secondary antibodies conjugated to Cy5 were from Jackson Immunoresearch; and secondary antibodies conjugated to DyLight 405 were from Rockland. DMSO, nocodazole, and taxol were from Sigma-Aldrich.

Western Blots and GST Pull-Downs. For analysis of EB protein expression, hippocampal neurons in culture from 3, 7, 10, 14, and 21 d in vitro (div) were solubilized in SDS sample buffer. Protein levels after normalization to β-tubulin were subjected to Western blot analysis. For GST pulldown assays, COS-1 cells transfected with ankG-GFP or ankB-GFP were solubilized in 10 mM Tris (pH 7.5), 150 mM NaCl, 1 mM EDTA, 1% Triton X-100, 0.1% deoxycholate, 0.1% BSA, and a complete protease inhibitor tablet (Roche) for 30 min at 4 °C and then were centrifuged at 14,000 × *g* for 15 min at 4 °C. The supernatant was incubated (4 h to overnight at 4 °C) with GST-EB3, GST-EB1, or GST previously coupled to glutathione Sepharose 4B following the manufacturer's instructions (GE Healthcare). The pulldown samples were resolved by SDS/PAGE and were immunoprobed using an anti-GFP antibody.

Surface Plasmon Resonance. AnkB (220 kDa) or ankG (190 kDa) was serially diluted twofold in running buffer. Samples were injected sequentially at 20 μL/min in increasing concentrations (range, 1–800 nM) using the Kinject command defining an association time of 180 s and a dissociation time of 60 s, except for the last injection, in which the dissociation time was extended to 15 min. The nonspecific signal (GST) was subtracted from the total signal (GST fusion protein), and control-run injections of buffer were performed in the same conditions before ankyrin injections and were subtracted for data analysis. Subtracted sensorgrams were globally fitted with the 1:1 titration kinetic binding model with Biacore software.

Immunofluorescence. After fixation (*Materials and Methods*), cells were blocked for nonspecific binding using 30-min incubation in ICC buffer (0.22% gelatin, 0.066% saponin in phosphate buffer). Cells were incubated for 75 min in ICC-diluted primary antibodies, rinsed and incubated with ICC-diluted secondary antibodies for 45 min. Coverslips were mounted in FluorSave reagent (Calbiochem).

Microscopy. Confocal imaging using a 63×, 1.4 NA oil objective also was used for a set of COS recruitment assay images. Illustrative images of cultured neurons were obtained using a 100×, NA 1.46 oil objective with a 1.6× magnifier and appropriate fluorescence filters. Overlapping tiles with adjusted Z-focus (3 × 3 or 4 × 4 images) were acquired automatically using the motorized stage.

Image Processing and Quantification. For quantifications, all measurements of intensities along the axon initial segment (AIS) and dendrites of neurons were made using NeuronJ software (13). For illustrations, overlapping tiles were stitched to obtain images with high resolution and a wide field of view (14). Assembled mosaics were processed using unsharp masking and contrast adjustment in Fiji.

Live Cell Imaging. Neurons were mounted in an open live-cell imaging chamber (Life Imaging Service), maintained at 37 °C, and imaged in osmolarity-adjusted extracellular medium (120 mM NaCl, 3 mM KCl, 2 mM CaCl2, 2 mM MgCl2, 10 mM glucose, 10 mM Hepes, 2% B27 supplement, pH 7.35, 260 mOsm). Time-lapse series (50- to 100-ms exposure, 0.5–2 s per frame) were acquired using a 100×, NA 1.46 oil objective and a 1.6× magnifier. Kymographs were generated from 1-pixel segmented lines traced along the AIS and dendrites, using the "Reslice" ImageJ command.

Fluorescence Recovery After Photobleaching Experiments. For fluorescence recovery after photobleaching (FRAP) experiments, AIS were revealed using live immunolabeling using an antibody against an extracellular epitope of neurofascin-186. Neurons were incubated 7 min at 37 °C with the primary antibody diluted in culture medium, followed by quick rinses and 7-min incubation at 37 °C with Alexa Fluor 555-conjugated secondary antibody diluted in culture medium. After rinses, neurons were mounted in the live imaging chamber. FRAP experiments were performed

at 37 °C on a DMI6000 microscope (Leica) with a 100×, NA 1.4 oil objective. Imaging was done using a spinning-disk system with a 473-nm laser (CSU22; Yokogawa) and FRAP was performed using a 100-mW 488-nm laser (Coherent) and a FRAP scanner system (Roper Scientific) piloted by MetaMorph (Molecular Devices). The FRAP laser was used for 5–10 ms at 100% power to bleach point regions (~1 μm wide) simultaneously in the AIS and proximal dendrites, reducing local fluorescence by 60–70%. Time-lapse images were acquired every 0.3–0.5 s using a QuantEM camera (Roper Scientific). Illumination intensity was set to prevent observational photobleaching (<10% in ~200 frames). Fluorescence signal was background subtracted and corrected for photobleaching. Best fits of FRAP recovery curves were generated in Prism software (Graphpad Software) according to the following equation: $F(t) = F_{max}[1-\exp(-K^*t)]$, where F_{max} is the plateau, i.e., the normalized maximal fluorescence limit for an infinite recovery time, and K is the inverse recovery time constant. The immobile population was defined as the difference between this recovery limit and total recovery, i.e., $(1 - F_{max})$.

1. Komarova Y, et al. (2005) EB1 and EB3 control CLIP dissociation from the ends of growing microtubules. *Mol Biol Cell* 16:5334–5345.
2. Hedstrom KL, et al. (2007) Neurofascin assembles a specialized extracellular matrix at the axon initial segment. *J Cell Biol* 178:875–886.
3. Zhang X, Bennett V (1998) Restriction of 480/270-kD ankyrin G to axon proximal segments requires multiple ankyrin G-specific domains. *J Cell Biol* 142:1571–1581.
4. Mohler PJ, Gramolini AO, Bennett V (2002) The ankyrin-B C-terminal domain determines activity of ankyrin-B/G chimeras in rescue of abnormal inositol 1,4,5-trisphosphate and ryanodine receptor distribution in ankyrin-B (–/–) neonatal cardiomyocytes. *J Biol Chem* 277:10599–10607.
5. Stepanova T, et al. (2003) Visualization of microtubule growth in cultured neurons via the use of EB3-GFP (end-binding protein 3-green fluorescent protein). *J Neurosci* 23: 2655–2664.
6. Komarova Y, et al. (2009) Mammalian end binding proteins control persistent microtubule growth. *J Cell Biol* 184:691–706.
7. Mimori-Kiyosue Y, Shiina N, Tsukita S (2000) The dynamic behavior of the APC-binding protein EB1 on the distal ends of microtubules. *Curr Biol* 10:865–868.
8. Geraldo S, Khanzada UK, Parsons M, Chilton JK, Gordon-Weeks PR (2008) Targeting of the F-actin-binding protein drebrin by the microtubule plus-tip protein EB3 is required for neuritogenesis. *Nat Cell Biol* 10:1181–1189.
9. Kizhatil K, et al. (2007) Ankyrin-G is a molecular partner of E-cadherin in epithelial cells and early embryos. *J Biol Chem* 282:26552–26561.
10. Abdi KM, Mohler PJ, Davis JQ, Bennett V (2006) Isoform specificity of ankyrin-B: A site in the divergent C-terminal domain is required for intramolecular association. *J Biol Chem* 281:5741–5749.
11. Coquelle FM, et al. (2002) LIS1, CLIP-170's key to the dynein/dynactin pathway. *Mol Cell Biol* 22:3089–3102.
12. Akhmanova A, et al. (2001) Clasps are CLIP-115 and -170 associating proteins involved in the regional regulation of microtubule dynamics in motile fibroblasts. *Cell* 104: 923–935.
13. Meijering E, et al. (2004) Design and validation of a tool for neurite tracing and analysis in fluorescence microscopy images. *Cytometry A* 58:167–176.
14. Preibisch S, Saalfeld S, Tomancak P (2009) Globally optimal stitching of tiled 3D microscopic image acquisitions. *Bioinformatics* 25:1463–1465.

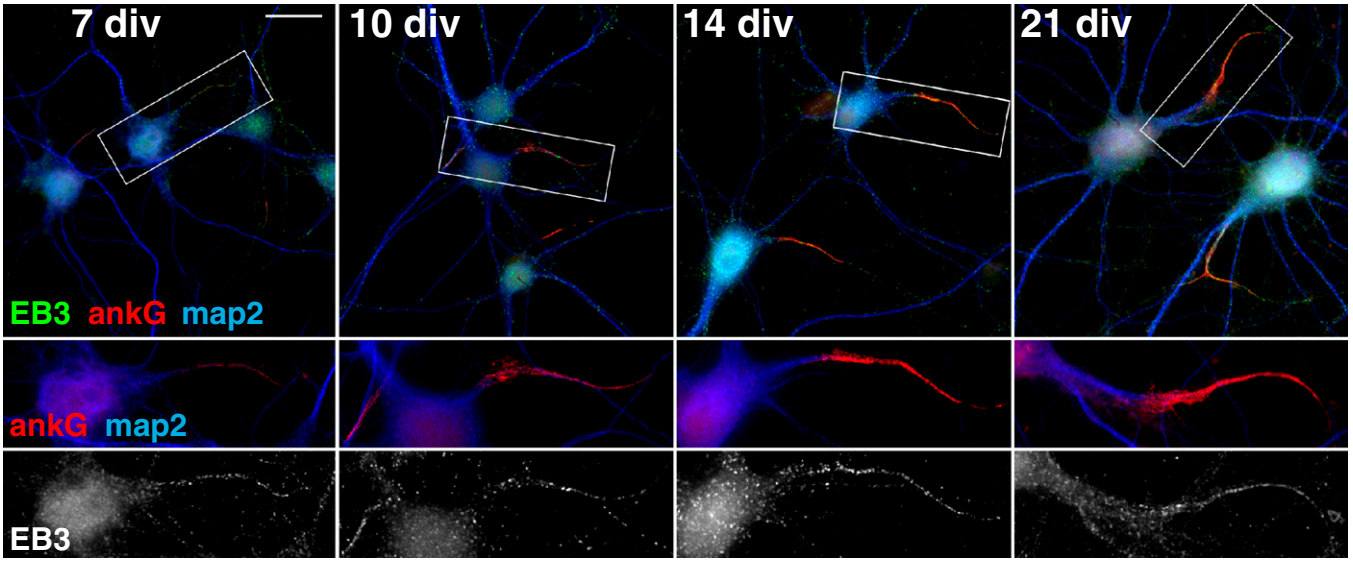

Fig. S1. Time-course of EB3 expression and AIS concentration in neurons. Shown are individual neurons corresponding to the quantifications shown in Fig. 1 *B* and *C*. As soon as EB3 is detected, it is concentrated in the AIS. EB3 is shown in green, ankG in red, and map2 in blue. (Scale bar: 20 μm.)

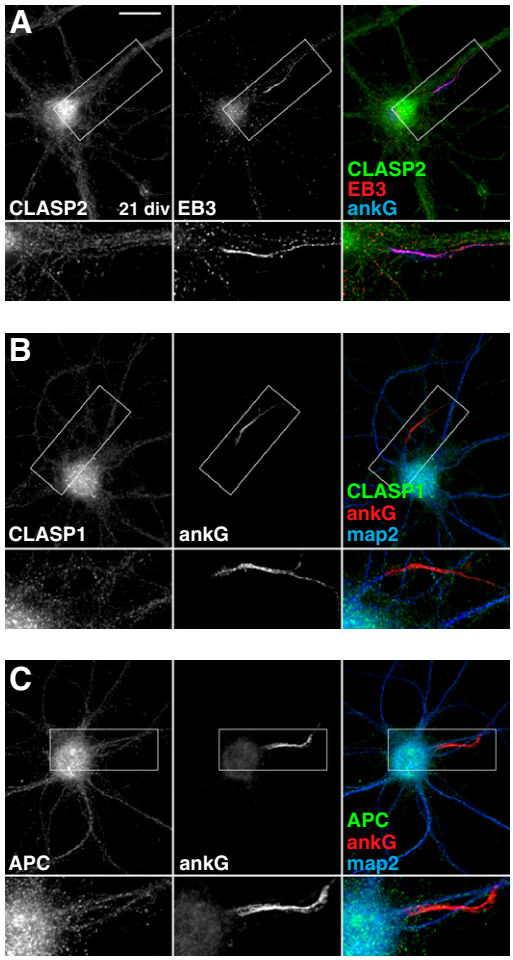

Fig. S2. EB-interacting positive end-tracking proteins (+TIPs) are excluded from the AIS. Immunolabeling for several EB protein-interacting +TIPS, supplementary to Fig. 1*D*. (*A*) Localization of CLASP2 in 21-div hippocampal neurons. CLASP2 puncta (green) are excluded from the AIS (ankG, blue), where EB3 (red) concentrates. (Scale bar: 10 μm.) (*B*) Localization CLASP1 in 21-div hippocampal neurons. CLASP1 puncta (green) localize in the somatodendritic compartment (map2, blue) but are excluded from the AIS (ankG, red). (*C*) Localization of APC in 21-div hippocampal neurons. APC puncta (green) localize in the somatodendritic compartment (map2, blue) and are not concentrated in the AIS (ankG, red).

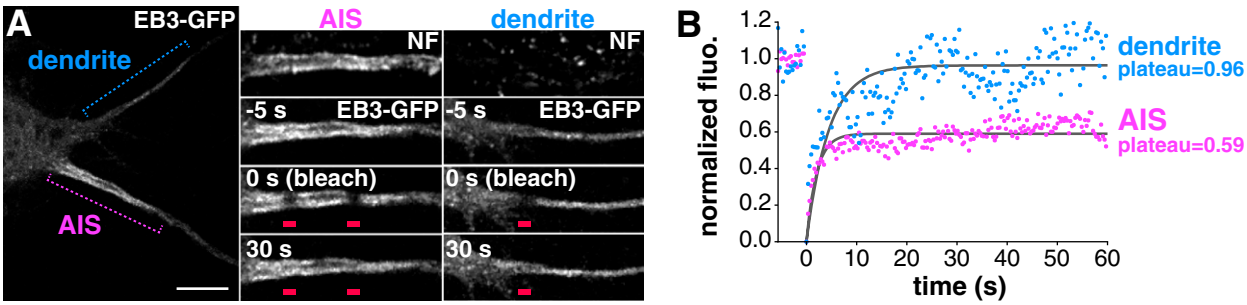

Fig. S3. Representative FRAP experiment. Shown is an Individual neuron corresponding to the FRAP experiments quantified in Fig. 2 *B* and *C*. (*A*) (*Left*) Spinning-disk microscopy image of an 8-div neuron 24 h after transfection with EB3-GFP. (Scale bar: 10 μm.) (*Right*) Zoomed boxes show the extracellular labeling for neurofascin-186 (NF) allowing to locate the AIS and time frames of EB3-GFP fluorescence taken before (−5 s), just after (0 s), and 25 s after (25 s) photobleaching of point regions in the AIS (purple) and a dendrite (blue). (*B*) Normalized fluorescence recovery curves of the neuron pictured in *A* averaged for the AIS regions (purple) and the dendritic regions (blue). The recovery is less complete in the AIS, as shown by the lower plateau calculated from a monoexponential fit of the recovery curves (gray).

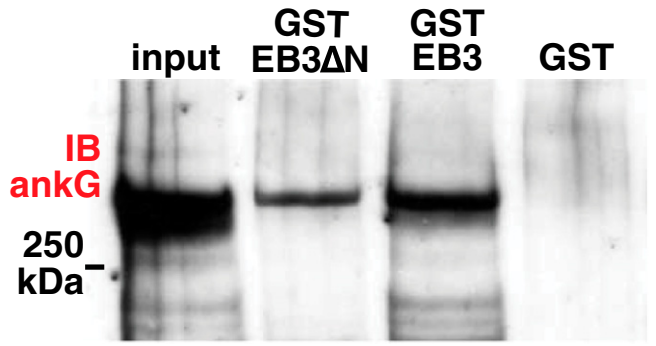

Fig. S4. Complete gel from GST-EB3 pulldown of ankG-GFP. Unprocessed gel corresponds to the experiment shown in Fig. 3*A*. GST-EB3ΔN (second lane), a GST fusion to a truncated EB3(196–281) lacking the MT-binding amino terminus, is able to bind ankG.

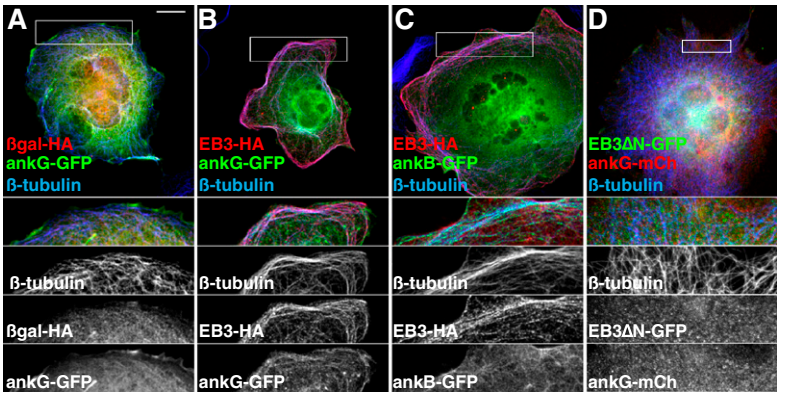

Fig. S5. EB3-HA recruits ankG, but not ankB, to microtubules (MTs), and EB3ΔN fails to localize to MTs. (*A*–*C*) Representative images of COS cells corresponding to the experiment quantified in Fig. 3*E*. (*A*) Expression of ankG-GFP (green) together with ßgal–HA (red) is unable to localize ankG to MTs (blue). (*B*) Coexpression of EB3-HA (red) with ankG-GFP (green) induces recruitment of ankG to MTs (blue). (Scale bar: 20 μm.) (*C*) In contrast, EB3-HA does not recruit ankB-GFP (green) to MTs (blue). (*D*) Truncated EB3Δ*N*-GFP lacking the MT-binding domain is unable to localize to MTs (blue) and does not recruit ankG-mCh (red) to MTs.

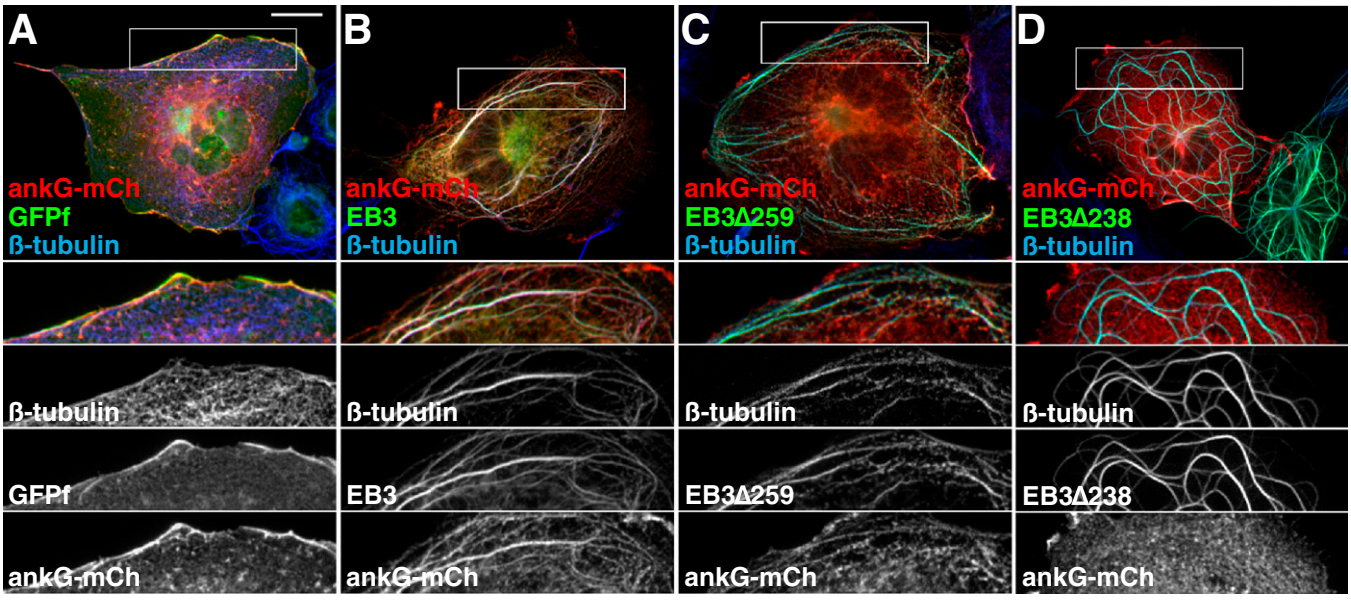

Fig. S6. Images showing behavior of EB3 mutant cells in the COS recruitment assay. Representative images of COS cells corresponding to the mutants quantified in Fig. 4*C* but not pictured in Fig. 4*D*. (*A*) ankG-mCh (red) does not localize to MTs (blue) when coexpressed with GFPf (green). (Scale bar: 20 μm.) (*B* and *C*) GFP-tagged full-length EB3 (green in *B*) and truncated EB3Δ259 (green in *C*) recruit ankG-mCh (red) to MTs (blue), in contrast to EB3Δ238 (green in *D*).

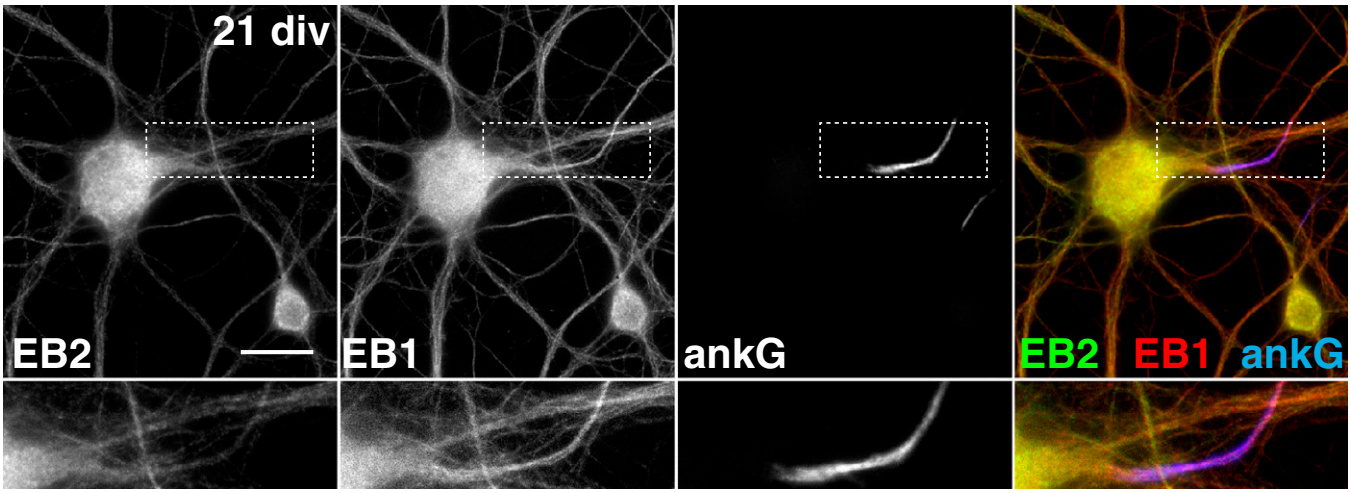

Fig. S7. EB2 does not localize to the AIS in mature neurons. Neuron (21 div) coimmunostained for EB1 and EB2. EB1 (red) is localized to axons and concentrates in the AIS. In contrast, EB2 (green) is found mainly in the soma and axons. AnkG (blue) labels the AIS. (Scale bar: 20 μm.)

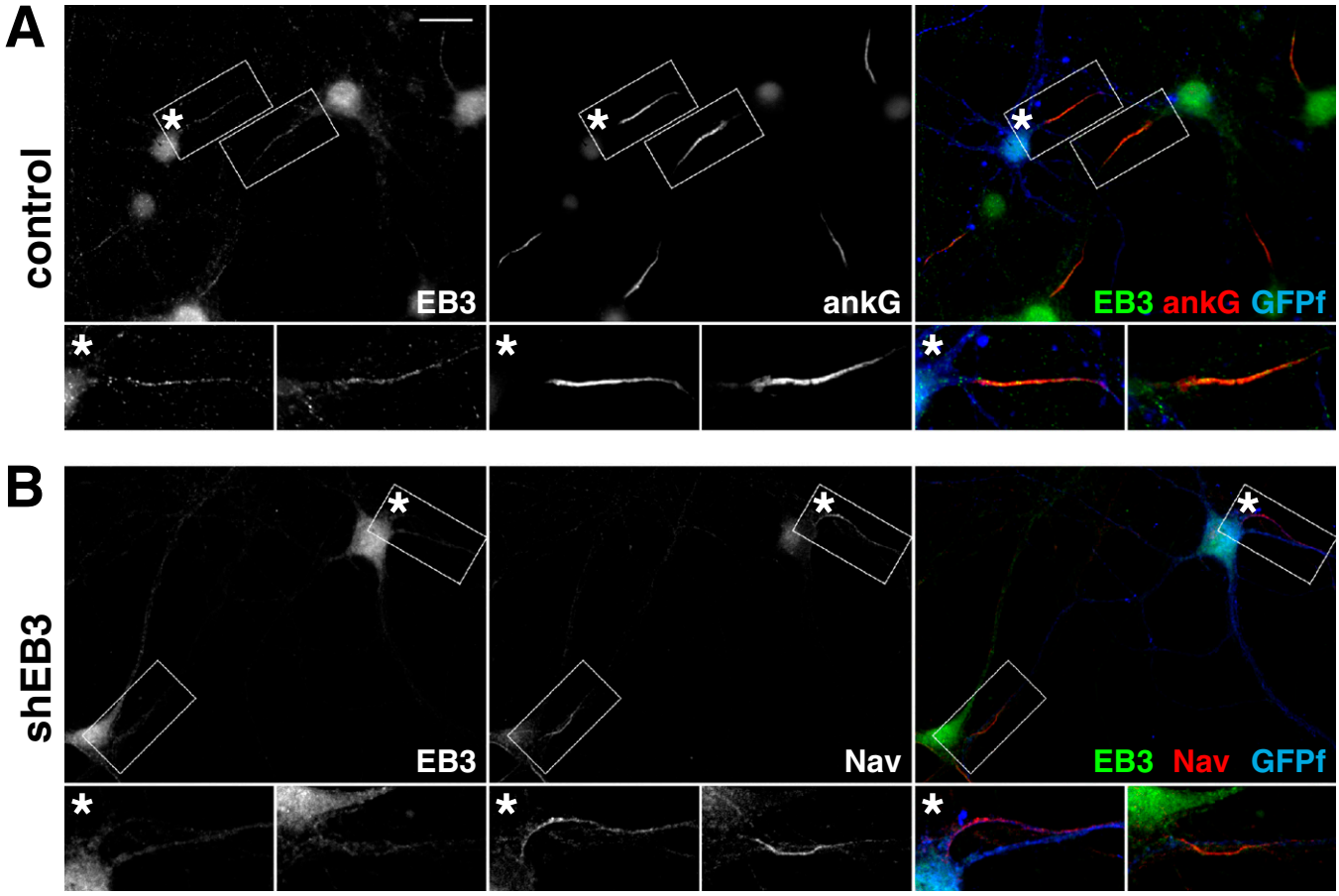

Fig. S8. Control shRNA plasmid does not perturb ankG concentration, and EB3 knockdown destabilizes Nav channels at the AIS. (*A*) Control condition corresponding to the experiment shown in Fig. 6*A*. Hippocampal neurons (16 div) 6 d after transfection with control plasmid lacking an shRNA cassette show unaltered ankG concentration in the AIS of a transfected neuron (asterisk-labeled box) compared with nontransfected neurons (unlabeled box). EB3 is shown in green, ankG in red, and GFPf in blue. (Scale bar: 20 μm.) (*B*) Representative image corresponding to the quantification shown in Fig. 6*C*. Hippocampal neurons (16 div) after 6 d of EB3 knockdown show a decreased concentration of Nav at the AIS of a transfected neuron (asterisk-labeled box) compared with nontransfected neurons (unlabeled box). EB3 is shown in green, Nav in red, and GFPf in blue.

Table S1. Kinetic parameters from surface plasmon resonance experiments for the interaction between ankyrins and GST-EB3 and GST-EB1 constructs

GST-EB	Ankyrin	Number of experiments	k_{on} (0.10^4 $M^{-1}s^{-1}$)	k_{off} (0.10^{-4} s^{-1})	K_d (0.10^{-9} M)
EB3	190-kDa ankG	15	7.3 ± 6.4	1.3 ± 1.6	1.7 ± 1.6
EB3	220-kDa ankB	3	NB	NB	NB
EB3Δ259	190-kDa ankG	8	11.5 ± 9.6	9.9 ± 19.9	1.1 ± 0.7
EB3Δ245	190-kDa ankG	5	NB	NB	NB
EB3Δ238	190-kDa ankG	4	NB	NB	NB
EB1	190-kDa ankG	3	11.8 ± 6.2	1.3 ± 0.5	1.4 ± 0.9

Quantitative parameters correspond to the experiments shown in Figs. 3*B* (EB3), 4*B* (EB3 mutants), and 5*E* (EB1). NB, no binding.

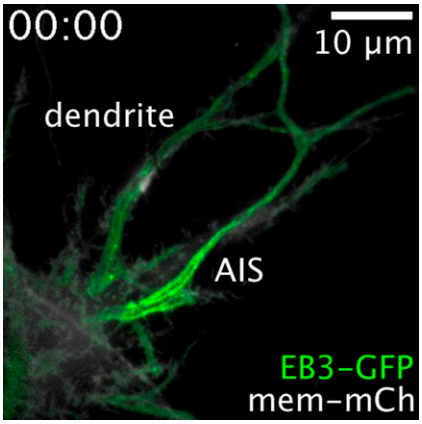

Movie S1. Dynamics of EB3-GFP in hippocampal neurons. This movie corresponds to the neuron shown in Fig. 2*A*. A 10-div hippocampal neuron 2 d after transfection with EB3-GFP (green) and membrane-targeted mCherry (mem-mCh; gray). Time-lapse images (every 0.5 s, total time 150 s) of EB3-GFP were taken using highly inclined laser illumination. The mem-mCh single image was taken using standard epifluorescence imaging.

Movie S1